Smoothed Particle Hydrodynamics simulations of the core-degenerate scenario for Type Ia supernovae

G. Aznar–Siguán[1,2], E. García–Berro[1,2][*], P. Lorén–Aguilar[3] N. Soker[4], A. Kashi[5]

[1] *Departament de Física Aplicada, Universitat Politècnica de Catalunya, c/Esteve Terrades 5, 08860 Castelldefels, Spain*
[2] *Institute for Space Studies of Catalonia, c/Gran Capità 2–4, Edif. Nexus 201, 08034 Barcelona, Spain*
[3] *School of Physics, University of Exeter, Stocker Road, Exeter EX4 4QL, UK*
[4] *Department of Physics, Technion Israel Institute of Technology, Haifa 32000, Israel*
[5] *Minnesota Institute for Astrophysics, University of Minnesota, 116 Church St. SE., Minneapolis, MN 55455, USA*

July 14, 2015

ABSTRACT

The core-degenerate (CD) scenario for type Ia supernovae (SN Ia) involves the merger of the hot core of an asymptotic giant branch (AGB) star and a white dwarf, and might contribute a non-negligible fraction of all thermonuclear supernovae. Despite its potential interest, very few studies, and based on only crude simplifications, have been devoted to investigate this possible scenario, compared with the large efforts invested to study some other scenarios. Here we perform the first three-dimensional simulations of the merger phase, and find that this process can lead to the formation of a massive white dwarf, as required by this scenario. We consider two situations, according to the mass of the circumbinary disk formed around the system during the final stages of the common envelope phase. If the disk is massive enough, the stars merge on a highly eccentric orbit. Otherwise, the merger occurs after the circumbinary disk has been ejected and gravitational wave radiation has brought the stars close enough for the secondary to overflow its Roche lobe radius. Not surprisingly, the overall characteristics of the merger remnants are similar to those found for the double-degenerate (DD) scenario, independently of the very different core temperature and of the orbits of the merging stars. They consist of a central massive white dwarf, surrounded by a hot, rapidly rotating corona and a thick debris region.

Key words: binaries: close — hydrodynamics — supernovae: general — stars: white dwarfs — stars: AGB and post-AGB

1 INTRODUCTION

Thermonuclear, or Type Ia supernovae (SNe Ia), originate from the explosion of carbon-oxygen white dwarfs — see, for instance Hillebrandt et al. (2013) and Ruiz-Lapuente (2014) for recent reviews on the explosion mechanisms and the different evolutionary channels — and are among the most luminous events in the universe. Moreover, since they arise from the detonation of white dwarfs with a relatively narrow range of masses, SNe Ia typically have similar intrinsic luminosities that can be conveniently standardized using the properties of the light curves, and consequently play a primary role in cosmology. However, the precise nature of the progenitor systems that give rise to SNe Ia remains still to be unveiled, and is a topic of active research. The fact that several peculiar SNe Ia have been discovered so far (e.g., Bildsten et al. 2007; Perets et al. 2010; Jordan et al. 2012;

Foley et al. 2013) suggests that different progenitors and/or explosion mechanisms could trigger such outbursts, resulting in normal and peculiar SNe Ia. For instance, the variety of peculiar SNe Ia and their range of properties, has led to explore sub-Chandrasekhar mass explosions — see, for instance, Wang, Justham & Han (2013) and Scalzo, Ruiter & Sim (2014).

It has long been suggested that a white dwarf in a binary system — with either another white dwarf — through the so-called double-degenerate (DD) scenario (Webbink 1984; Iben & Tutukov 1984) — or a main-sequence or red giant companion — through the single-degenerate (SD) scenario (Whelan & Iben 1973; Nomoto 1982; Han & Podsiadlowski 2004) — could give rise to a SN Ia event. More recent scenarios — see the reviews of Wang & Han (2012) and Maoz, Mannucci & Nelemans (2014) — are variants of the two previously mentioned ones, and include the double detonation scenario, where helium-rich material is accreted by the carbon-oxygen white dwarf (e.g., Shen & Bildsten 2009;

[*] Corresponding author, email: enrique.garcia-berro@upc.edu

Ruiter et al. 2011), the double white dwarf collision scenario (Raskin et al. 2009; Rosswog et al. 2009; Thompson 2011; Kushnir et al. 2013), and the core-degenerate (CD) scenario (Sparks & Stecher 1974; Livio & Riess 2003; Kashi & Soker 2011; Ilkov & Soker 2012, 2013; Soker et al. 2013) to be studied here. Within the CD scenario the white dwarf merges with the hot core of a massive asymptotic giant branch (AGB) star (Livio & Riess 2003; Kashi & Soker 2011; Ilkov & Soker 2012, 2013). In a recent paper Tsebrenko & Soker (2015b) argue that approximately 20%, and likely many more, of all SNe Ia come from the CD scenario. However, Zhou et al. (2015) and Meng & Yang (2012) using Monte Carlo binary population synthesis codes concluded that the fraction is only 2–10%, but another recent population synthesis study suggests that the merger of the core of an AGB star and a white dwarf can indeed be very common (Briggs et al. 2015). A table summarizing these scenarios with their main advantages and drawbacks can be found in Tsebrenko & Soker (2015b). To these we add a note on the recently proposed singly-evolved star (SES) scenario (Chiosi et al. 2015).

The DD and the CD scenarios share many similarities, and in particular they have a common initial evolutionary path. Typically, in a low- or intermediate-mass binary system the more massive (primary) component fills its Roche lobe while crossing the Hertzsprung gap in the color-magnitude diagram and the mass transfer episode is stable. The primary star then evolves into a carbon-oxygen white dwarf. Later, the initially secondary star fills its Roche lobe when it becomes an evolved giant star. This time the combination of a deep convective envelope and an extreme mass ratio causes an unstable mass transfer episode from the giant to the white dwarf and a common envelope is formed. In the DD channel the common envelope is entirely ejected and a final binary system made of two white dwarfs is obtained, where the second white dwarf formed is normally the more massive one (Webbink 1984). Gravitational wave radiation finally brings both white dwarfs closer and a merger occurs. In the CD channel the merger occurs shortly after the common envelope phase.

Note, however, that there are two significant differences between the DD and the CD scenarios. In a DD merger both white dwarfs are brought together by gravitational wave radiation, a process which lasts for a long time. Consequently, it is expected that both components of the binary system are cool, and have nearly circular orbits. Moreover, it is also foreseen that both white dwarfs will be synchronized. In contrast, in the CD scenario the merger of both stars is triggered by the interaction with the circumbinary disk. In particular, in the CD scenario during the final stages of the common envelope phase, $\sim 10\%$ of the common envelope remains bound to the binary system formed by the AGB star and the companion white dwarf, forming a circumbinary disk — see Kashi & Soker (2011), and references therein. Consequently, it turns out that in a sizable number of cases as the binary system transfers angular momentum to the circumbinary disk, the separation of the pair decreases and the eccentricity of the system increases (Artymowicz et al. 1991) while the core of the AGB star is still hot (Kashi & Soker 2011), favoring a merger at the end of the common envelope phase or a short time after, during the planetary nebula phase. However, it might be also possible that, if the

circumbinary disk is not massive enough, the merger takes place after the circumbinary disk has been already ejected. In this case the driver of the merger is again the emission of gravitational waves, so the orbits will have a small eccentricity and the temperature of the core of the post-AGB star will be low. In summary, in the CD scenario a considerably large range of eccentricities of the binary system and of temperatures of the naked core of the AGB star are expected, at odds with what is foreseen for the DD channel.

While several simulations of the DD progenitor channel have been already performed over the last two decades (Benz et al. 1990; Segretain, Chabrier & Mochkovitch 1997; Guerrero, García-Berro & Isern 2004; Yoon, Podsiadlowski & Rosswog 2007; Lorén-Aguilar, Isern & García-Berro 2009; Pakmor et al. 2010; Dan et al. 2011; Raskin et al. 2014), no full three-dimensional simulation of the CD scenario has been done so far. The present paper aims at filling this gap, and it is organized as follows. In Section 2 we discuss the initial conditions considered to simulate the CD scenario. It is followed by Section 3, where we briefly explain the numerical techniques used in this paper. In Section 4 we describe in depth the results of our simulations. Finally, in Section 5 we summarize our main findings, and we draw our conclusions.

2   INITIAL CONDITIONS

2.1   The final phase of the common envelope

Kashi & Soker (2011) estimated that during the last stages of the common envelope phase, between $\sim 1\%$ and 10% of the ejected envelope remains bound to the binary system composed of the cold white dwarf and the hot core of the AGB star. They furthermore suggested that, due to angular momentum conservation and further interaction of the remaining common envelope with the binary system, the fallback material forms a circumbinary disk around the binary. This newly formed disk would later interact with the binary system, thus reducing the orbital separation of the pair much more than what it was reduced during the dynamical phase where the common envelope is ejected, while the eccentricity of the binary system would increase. Using the results of Artymowicz et al. (1991), Kashi & Soker (2011) obtained the rate at which the semimajor axis decreases and the rate at which the eccentricity of the orbit increases. In addition, they also took into account the rate at which the circumbinary disk losses mass during the interaction.

Kashi & Soker (2011) found that the final values of the orbital parameters critically depend on the amount of matter ejected from the system through disk winds. Specifically, they found that for disks with masses $M_{disk} \gtrsim 0.12(M_{core} + M_{WD})$ — where M_{disk}, M_{core}, and M_{WD} are, respectively, the masses of the disk, the core of the AGB star and the white dwarf — the circumbinary disk-binary interaction leads to a merger if the speed of the disk wind is the escape velocity. For the particular case studied by Kashi & Soker (2011), where $M_{WD} = 0.6\,M_\odot$, $M_{core} = 0.77\,M_\odot$ and $M_{env} = 4.23\,M_\odot$, the mass of the disk amounts to $\sim 4\%$ of the mass of the envelope. They also found that for less massive circumbinary disks the separation is not reduced enough to result in a merger during the interaction. In these cases, gravitational wave radiation will reduce the orbital
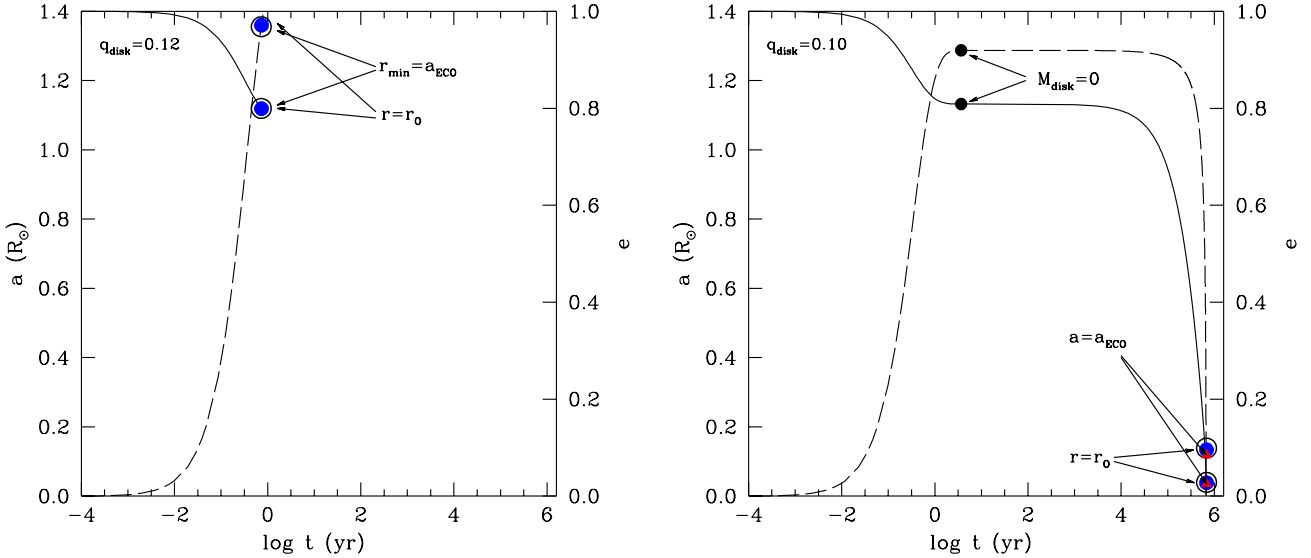
Figure 1. Evolution of the orbital parameters of the binary system formed by an AGB star and a white dwarf during its interaction with the circumbinary disk, once a large fraction of the envelope of the AGB star has been ejected. The left panel shows the case in which a massive circumbinary disk with $q_{\rm disk} = 0.12$ is adopted, whereas the right panel the case in which $q_{\rm disk} = 0.10$ is considered — see text for details. The solid lines and left scale show the evolution of the semimajor axis (a), and the dashed lines and the right scale display that of the eccentricity (e). The hollow, large circles indicate the point at which the minimum orbital distance is such that the secondary would overflow its Roche lobe for the equivalent circular orbit, $r_{\rm min} = a(1 - e) = a_{\rm ECO}$, whereas the blue solid symbols show the orbital distance a when the secondary white dwarf fills its Roche-lobe radius in our simulations, $r = r_{\rm O}$. Finally, for the right panel, the point at which the semi-major axis of the binary system equals the distance at which the secondary reaches the Roche-lobe radius for the equivalent circular orbit, $a = a_{\rm ECO}$ is indicated by a triangle. Also in this panel the time at which the circumbinary disk has been totally ejected is indicated by the solid black circles.

separation, a, and the eccentricity, e, further. Consequently, the final merger would occur when the orbit of the binary system is almost circular. Hence, in these cases it turns out that the orbital separation, a, and the distance at closest approach, $r_{\rm min} = a(1 - e)$, are very similar. The first mass transfer episode occurs when $r_{\rm min} < r_{\rm O}$ but $a > r_{\rm O}$, being $r_{\rm O}$ the distance between the two stars when the secondary overflows its Roche lobe radius in our numerical simulations. It is convenient to define here an equivalent circular orbit, which is the circular orbit for which $R_2 \simeq R_{\rm L}$, where R_2 is the radius of the secondary star, and $R_{\rm L}$ is computed using the expression of Eggleton (1983). We call the semi-major axis of this orbit $a_{\rm ECO}$. Moreover, since the timescale for gravitational wave emission is long, the core of the AGB star would be cold (Kashi & Soker 2011). Note, however, that although the procedure detailed in Kashi & Soker (2011) takes into account the tidal interaction during the common envelope phase, to compute the orbital parameters of our system at which our SPH simulations start (see below) we did not take into account tidal effects once the circumbinary disk has been totally ejected from the system.

2.2 Orbital parameters

We compute the evolution of the orbital parameters of the binary system before the merger occurs following closely the procedure of Kashi & Soker (2011). In particular, we consider the same binary as Kashi & Soker (2011) and we adopt two different disk masses. Writing

$$M_{\rm disk} = q_{\rm disk}(M_{\rm core} + M_{\rm WD}), \tag{1}$$

we adopt as reference cases $q_{\rm disk} = 0.12$ — a disk with a mass just over the critical one — and $q_{\rm disk} = 0.10$ — a low-mass one. When $q_{\rm disk} = 0.12$ the merger occurs just before the disk is totally ejected from the system. Hence, the merger would occur when the orbit of the binary system is still highly eccentric, and moreover the core of the AGB star would still be hot, while when $q_{\rm disk} = 0.10$ the merger occurs long after the circumbinary disk has been totally ejected from the system, and hence the orbit will be nearly circular, and the core of the AGB ill be cold.

The time evolution of the orbital parameters for $q_{\rm disk} = 0.12$ is displayed in the left panel of Fig. 1, where we show the evolution of both the orbital separation (solid line, left scale), and of the eccentricity (dashed line, right scale). The large, hollow circles correspond to the time instant at which the periastron distance is such that the radius of the secondary would equal the Roche-lobe radius ($R_2 = R_{\rm L}$) for the equivalent circular orbit, while the solid, blue circles show the point at which the mass transfer episode begins — see below for details about the mass transfer episode. Note that both times are almost coincidential. For this disk, the merger occurs at $t \sim 270$ days after the common envelope is ejected.

The equivalent diagram for the case in which $q_{\rm disk} = 0.10$ is shown in the right panel of Fig. 1. In this case, the disk has been totally ejected at early times (the time at

which this occurs is represented using black, solid circles in this figure). For a relatively long time interval the orbital separation and the eccentricity of the pair remain almost constant, but as time goes on the emission of gravitational waves progressively decreases the orbital distance and the eccentricity of the pair, being faster for times just before the merger begins. Eventually, at approximately 6×10^5 years after the common envelope of the system is ejected both stars merge. As in the previous case we also show in this panel the points where $R_2 = R_L$ for the equivalent circular orbit, and the points at which the merger starts. Additionally, in this panel we also show using red triangles the times for which the semi-major axis equals the distance at which the secondary reaches the Roche lobe radius for the equivalent circular orbit ($a = a_{ECO}$). Note that in this case the eccentricity is small ($e \sim 0.1$) and that we expect that, given the very long timescale of gravitational wave emission, the post-AGB star will have a cold core. In cases where merger takes place within several times 10^5 yr, the SN Ia ejecta might catch up with the ejected common envelope, that once was a planetary nebula. This "SN Ia Inside a PN" is termed a SNIP (Tsebrenko & Soker 2015b,a).

2.3 The temperature of the AGB core

For the sake of completeness for each of the cases described earlier we perform two simulations. For the first of these simulations we adopt a low temperature for the isothermal core of the AGB star ($T = 10^6$ K), while for the second we adopt a hot core ($T = 10^8$ K). Admittedly, these are first order approximations, since realistic temperature profiles should be adopted. However, given that the degeneracy of typical AGB cores is high we expect that the influence of the adopted temperature profiles on the evolution of the merger will be small. The white dwarf is always cold, and for it we adopt $T = 10^6$ K. The adopted temperature has an effect on the initial configuration of the core of the AGB star (of mass $M_{core} = 0.77\,M_{\odot}$). The radii are $R_{core} \simeq 1.02 \times 10^{-2}\,R_{\odot}$ and $R_{core} \simeq 9.33 \times 10^{-3}\,R_{\odot}$, and the central densities are $\rho_c^{core} \simeq 6.83 \times 10^6$ g cm^{-3} and $\rho_c^{core} \simeq 7.07 \times 10^6$ g cm^{-3}, for the hot and cold cores, respectively. Note that these differences are small, of the order of a few percents, and thus given the approximations adopted in this work, have limited effects on the dynamical evolution of the merger, and on the question of whether there is an ignition upon merger (Yoon, Podsiadlowski & Rosswog 2007).

3 NUMERICAL SETUP

Both the white dwarf and the core of the AGB star are made of equal mass fractions of carbon and oxygen, with flat profiles. We would like to mention here that the outer helium layer of $\sim 0.01\,M_{\odot}$ surrounding the cores of the white dwarf and of the AGB star could be potentially important for the evolution of the merger. However, with the number of particles adopted in our SPH simulations this helium shell it is practically unresolvable and difficult to follow its evolution numerically.

The SPH code used in this work is an optimized and updated version of the code used by Guerrero, García-Berro & Isern (2004) and later by Lorén-Aguilar, Isern &

García-Berro (2009), Lorén-Aguilar, Isern & García-Berro (2010) and Aznar-Siguán et al. (2013) to simulate double-degenerate mergers. This code has been extensively described in those works. Consequently, here we will only summarize its more important characteristics.

Our SPH code is fully parallel, and allows to run simulations with a large number of particles in a reasonable time. We use the standard cubic spline kernel of Monaghan & Lattanzio (1985). The gravitational interaction is also softened using this kernel (Hernquist & Katz 1989). The search of neighbors and the evaluation of the gravitational forces are performed using an octree (Barnes & Hut 1986). The iteration method of Price & Monaghan (2007) is used to compute the smoothing lengths. To deal with shocks we employ a prescription for the artificial viscosity based in Riemann solvers (Monaghan 1997), and the variable viscosity parameters of Morris & Monaghan (1997) are employed. Additionally, to suppress artificial viscosity forces in pure shear flows the viscosity switch of Balsara (1995) is also used. As explained in detail in Aznar-Siguán et al. (2013), we follow the evolution of both the internal energy and of the temperature to ensure a reliable evolution of the temperature in a degenerate gas. The thermodynamic properties of matter are computed using the Helmholtz equation of state (Timmes & Swesty 2000). Finally, the nuclear network adopted here incorporates 14 nuclei. The reactions considered in this work are captures of α particles, and the associated back reactions, the fusion of two carbon nuclei and the reaction between carbon and oxygen nuclei. All the thermonuclear reaction rates were taken from the REACLIB data base (Cyburt et al. 2010). Neutrino losses were also included, being the corresponding rates those of Itoh et al. (1996).

As mentioned before, the first mass transfer episode begins when $r_{min} < r_O < a$. To obtain reliable configurations when both stars are at closest approach we proceeded as follows. We first relaxed independent configurations for each of the stars of the binary system and we placed them at the apastron in a counterclockwise orbit. We then evolved the system in the corotating frame to obtain equilibrium configurations at this distance. Once this relaxation process was finished, we started the simulations in the inertial reference frame. In a first set of preliminary simulations we explored at which distance the mass transfer episode ensues. This is done employing a reduced number of particles ($\sim 2 \times 10^4$ for each star). Once we know which are the orbital separation and the eccentricity of the orbit for which we obtain a Roche-lobe overflow we computed a second set of simulations with enhanced resolution. Since for highly eccentric orbits both stars are initially separated by very large distance, to save computing time in this second set of simulations we first followed the evolution of the system employing the reduced resolution and, once the stars had completed one quarter of the orbit, these low-resolution simulations were stopped and both stars were remapped using a large number of SPH particles (a factor of 10 larger). We then resumed the simulations with this enhanced resolution. This was done because for systems with large eccentricities the computing load required to follow an uninteresting phase of the orbital evolution of the pair is exceedingly large.
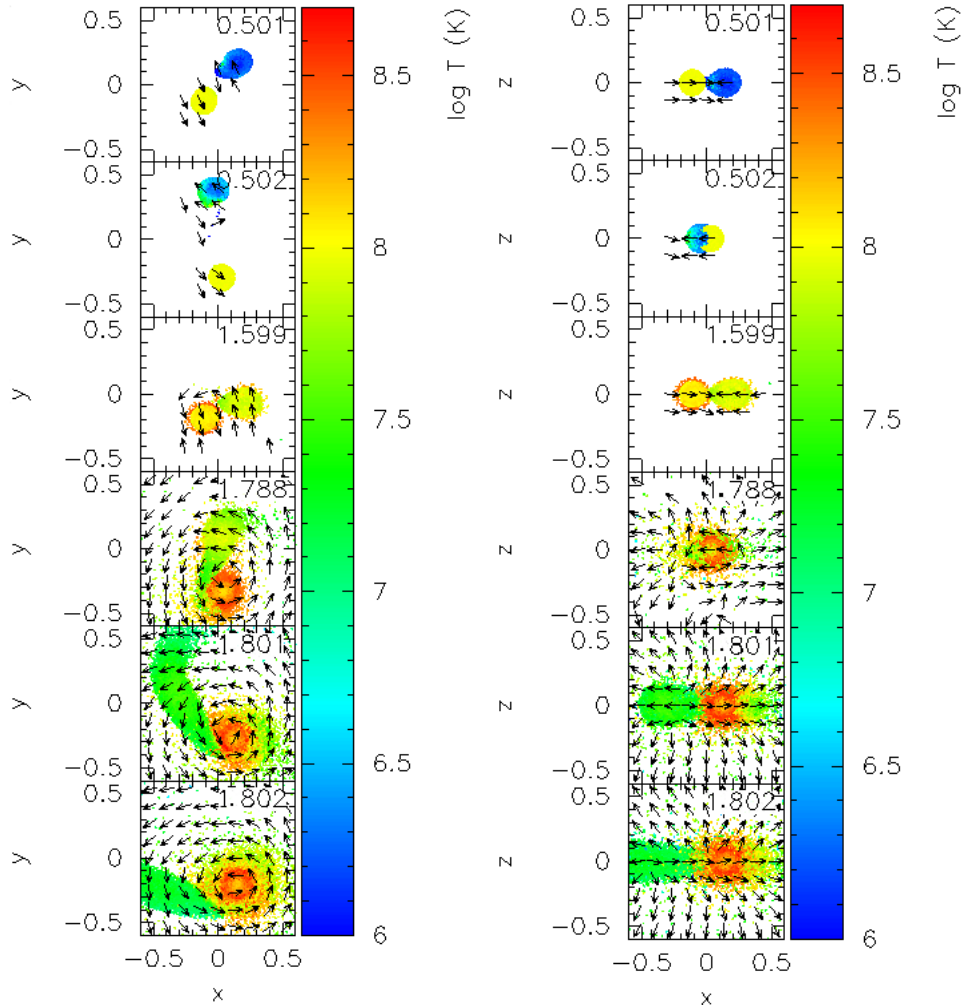
Figure 2. Evolution of the binary system for selected stages of the merger, as described in the main text, in the equatorial (left) and meridional (right) planes, for the case in which a hot core of the AGB star is adopted and for $q_{\mathrm{disk}} = 0.12$. The color scale shows the logarithm of the temperature, whereas the x, y and z axes are in units of $0.1\,R_\odot$. The arrows show the direction of the velocity field, but not its magnitude, in the corresponding plane. Each panel is labelled with the corresponding time in units of the initial binary period, $T_0 = 10,126$ s. The white dwarf is the object located initially at the right, and later is destroyed. These figures have been done using the visualization tool SPLASH (Price 2007). See the online edition of the journal for a color version of this figure.

4 RESULTS

As discussed earlier, in this paper we simulate four different configurations for the binary system. In all cases the mass of the core of the AGB star and the white dwarf are, respectively, $0.77\,M_\odot$ and $0.60\,M_\odot$. The first configuration corresponds to a binary system that has a disk with a mass ratio equal to the critical one of $q_{\mathrm{disk}} = 0.12$ (see equation 1), while for the second one we have chosen a disk with a mass ratio of $q_{\mathrm{disk}} = 0.1$, which is below the critical value. For each one of these cases we have studied the coalescence when the temperature of the core of the AGB star is high ($T = 10^8$ K) and low ($T = 10^6$ K).

For the highly eccentric orbit that results when $q_{\mathrm{disk}} = 0.12$ is adopted, the first mass transfer from the white dwarf to the core of the AGB star occurs when the distance between both components of the binary system at closest approach is $r_{\min} = 0.90\,a_{\mathrm{ECO}}$, where a_{ECO} has been defined previously in section 2.1 as the radius of a circular orbit for

which the white dwarf overflows its Roche lobe. In computing this orbital distance the classical analytical expresion of Eggleton (1983) for the Roche lobe radius R_{L} was used. Note that this expression does not take into account tidal deformations, and is only valid for circular orbits, while the orbits of the binary systems studied here are elliptical and our stars are tidally distorted. At this time the semimajor axis is $a = 1.12\,R_\odot$ and the eccentricity is $e = 0.97$. For the less massive disk with $q_{\mathrm{disk}} = 0.10$ the merger begins when $a = 0.038\,R_\odot$ and the eccentricity of the orbit is small $e = 0.095$. Specifically, the merger occurs when $r_{\min} = 0.98\,a_{\mathrm{ECO}}$. Fig 1 illustrates all this. Particularly relevant for the discussion of our results are the values of the respective initial periods. For the case of the system with $q_{\mathrm{disk}} = 0.12$ the initial orbital period is $T_0 \simeq 10,126$ s, while for the case in which $q_{\mathrm{disk}} = 0.10$ is used the initial period is significantly shorter, $T_0 \simeq 65$ s.
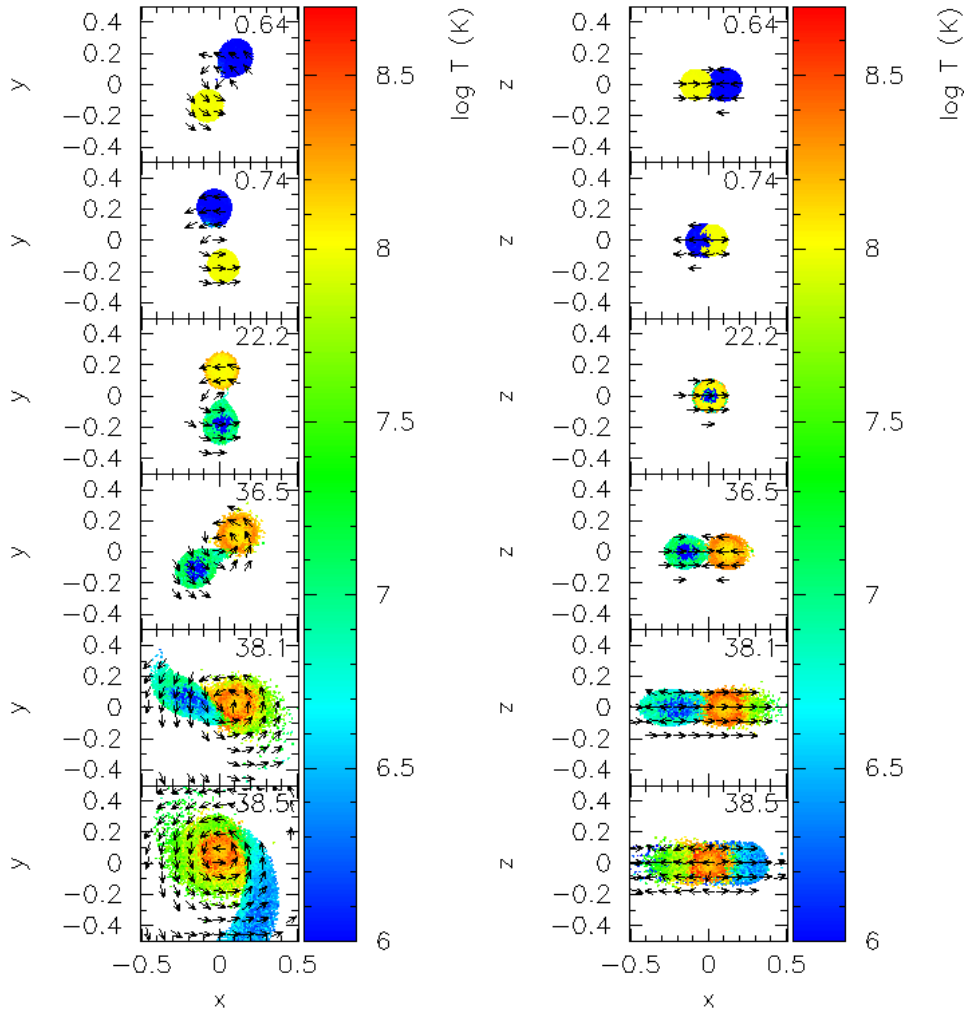
Figure 3. Same as Fig. 2, but for $q_{\rm disk} = 0.10$. In this case the initial orbital period is $T_0 = 65$ s. See the online edition of the journal for a color version of this figure.

4.1 Evolution of the merger

Fig. 2 shows the time evolution of the binary system during the merger for the case in which the temperature of the AGB core is 10^8 K and for $q_{\rm disk} = 0.12$. Shown are the positions of the SPH particles and their color-coded temperatures. The left column shows the evolution in the orbital plane and the right column in the meridional plane, respectively. In Fig. 3 we present the results in the same setting for the case in which $q_{\rm disk} = 0.10$ is adopted. The white dwarf is the object located initially at the right, and later is destroyed, while the core of the AGB star is initially located at the left.

The top panels of Figs. 2 and 3 are at the initial stages of the merger, at times $t/T_0 \simeq 0.501$ for $q_{\rm disk} = 0.12$, and $t/T_0 \simeq 0.640$ for $q_{\rm disk} = 0.10$, respectively. We remind that the orbital periods are $T_0 = 10,126$ s for $q_{\rm disk} = 0.12$, and $T_0 = 65$ s for $q_{\rm disk} = 0.10$, respectively. As can be seen the white dwarf is significantly deformed, due to tidal interactions, the deformation being larger for the case of an eccentric orbit (Fig. 2). For the second row of panels we have chosen slightly larger times, $t/T_0 \simeq 0.502$ and $t/T_0 \simeq 0.74$, respectively, and show that tidal deformations close to periastron are much larger for eccentric mergers. This leads

to a faster heating of the external layers of the secondary star. The third rows show the systems when the system has evolved through several passages trough the periastron. For $q_{\rm disk} = 0.12$ (Fig. 2) we have chosen the sixth mass transfer episode and for $q_{\rm disk} = 0.10$ (Fig. 3) the twenty-third one. These correspond to times $t/T_0 \simeq 1.599$ and $t/T_0 \simeq 22.2$, respectively. As can be seen, at these evolutionary stages in both cases the secondary (the white dwarf) has increased its temperature, and more mass has been accumulated on the primary core.

The fourth rows of Figs. 2 and 3, at times $t/T_0 \simeq 1.788$ and $t/T_0 \simeq 36.5$ respectively, display the situation during the last orbit, just before the secondary white dwarfs are completely disrupted by the cores of the AGB stars. At this point, for $q_{\rm disk} = 0.12$ the white dwarf still keeps $\approx 80\%$ of its initial mass, while for $q = 0.10$ this percentage is somewhat larger, $\approx 90\%$. The fifth rows correspond to a time close to that at which the peak temperature is reached, which happens during the final infall of the secondary star onto the core of the AGB star. Specifically, we have chosen $t/T_0 \simeq 1.801$ and $t/T_0 \simeq 38.1$, respectively. As it will be discussed in more detail later, for $q_{\rm disk} = 0.12$ these temperatures are higher than for $q_{\rm disk} = 0.10$. The reason for this is
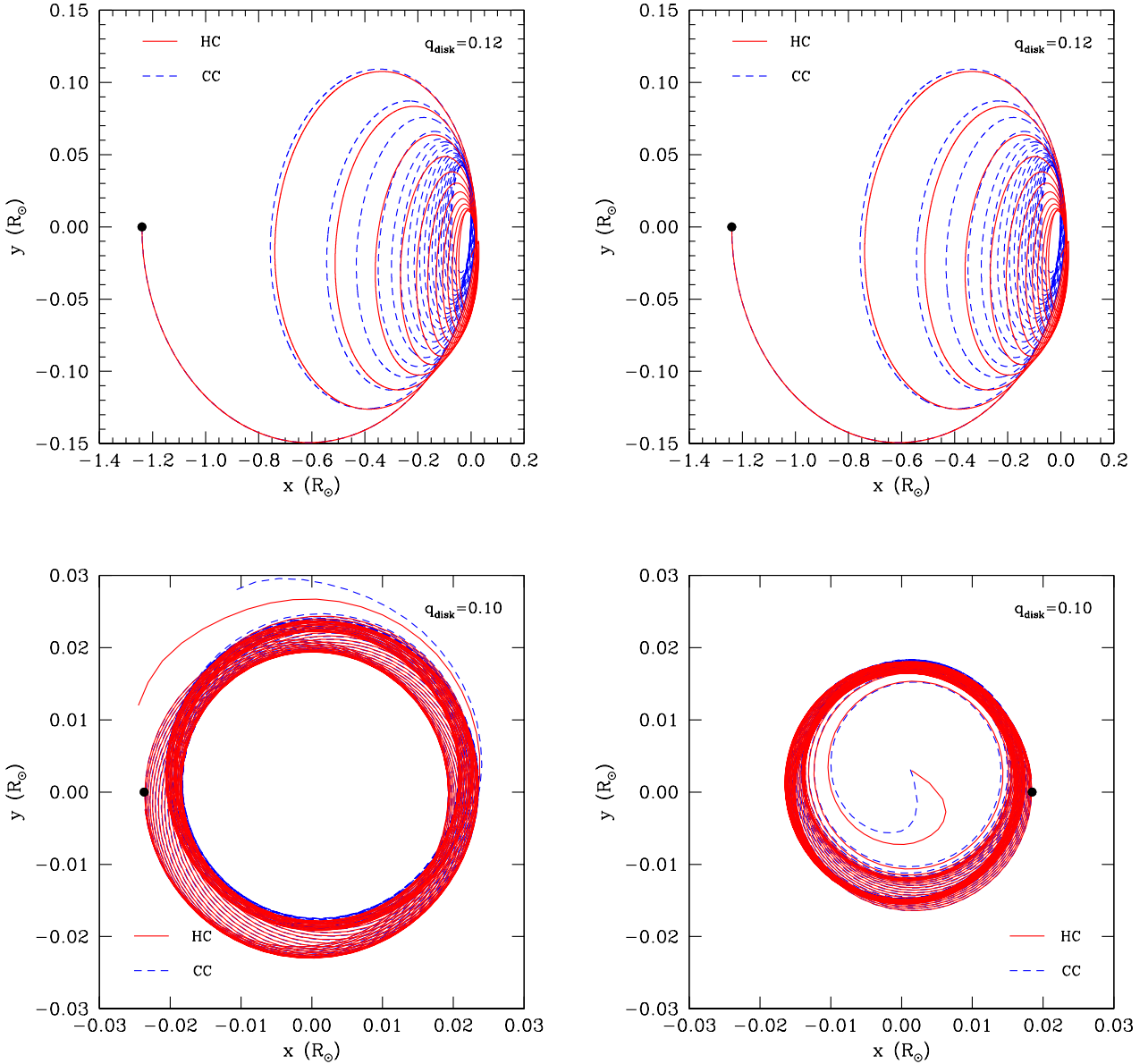
Figure 4. Trajectories of the centers of mass of the white dwarfs (left panel) and cores of the AGB stars (right panel) for the case in which $q_{disk} = 0.12$ is adopted (top panels) and that in which $q_{disk} = 0.10$ is employed (bottom panels). The blue dashed lines correspond to the case in which a cold AGB core is adopted, and the red solid lines to that in which a hot core is assumed. The solid black circles indicate the initial positions of both stars for each of the panels.

twofold. First, the material of the white dwarf is hotter for $q_{disk} = 0.12$, a consequence of the previous evolution. The second reason is that in this case the matter of the disrupted white dwarf falls onto the primary star with a much larger radial velocity than for $q_{disk} = 0.10$. Consequently, matter is compressed more violently in this case. Finally, the last rows show the systems at late times. We have chosen times $t/T_0 \simeq 1.802$ and $t/T_0 \simeq 38.5$, respectively. As can be seen, the material of the completely disrupted secondary white dwarf is spiralling around the primary star.

A general feature of our simulations is that the secondary star, the white dwarf, is totally disrupted after sev-

eral periastron passages. In each of these periastron passages mass is transferred in a relatively gentle way. Accordingly, in all cases the density and temperature conditions for a detonation to develop are not met. As can be seen in Figs. 2 and 3, in none of the cases the peak temperature reaches 10^9 K, and hence, although nuclear reactions play a role, a powerful explosion does not occur. Nevertheless, the helium shells of the white dwarf and the core of the AGB star can play a role in inducing a detonation. However, none of the studies of merging white dwarfs performed so far (Guillochon et al. 2010; Townsley, Moore & Bildsten 2012; Moore, Townsley & Bildsten 2013; Pakmor et al. 2013; Shen & Moore 2014)
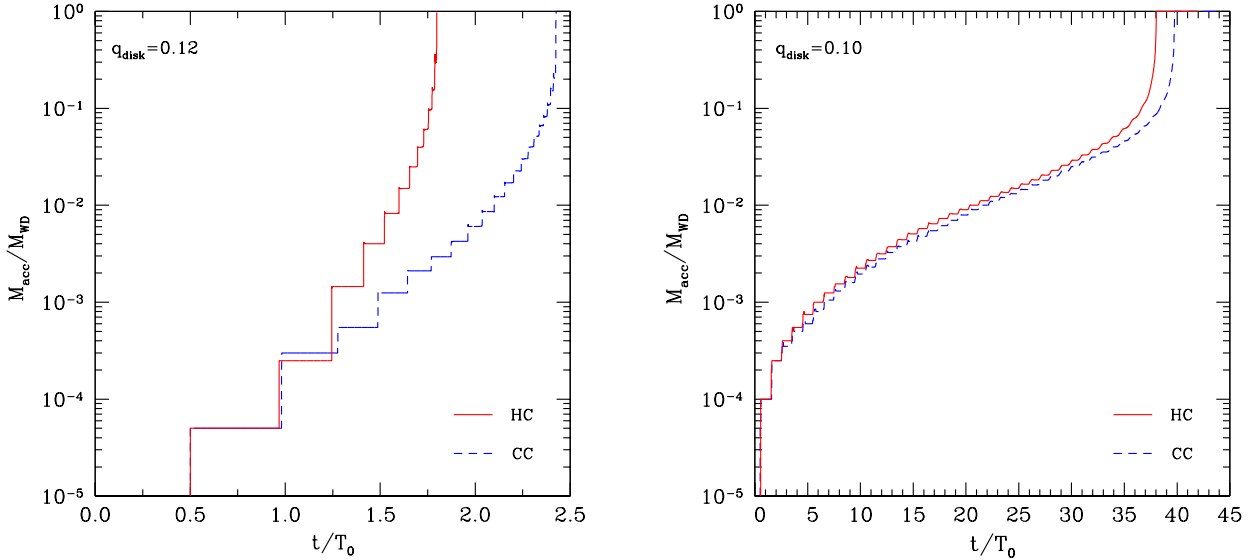
Figure 5. Mass accreted by the AGB core as a function of time, expressed in terms of the initial orbital period. The left panel corresponds to $q_{\mathrm{disk}} = 0.12$, while the right displays the case in which $q_{\mathrm{disk}} = 0.10$. Each step in these panels corresponds to a periastron passage. The total time span is $\simeq 25,315$ s for the left panel, and $\simeq 2,925$ s for the right one.

has been able to self-consistently evolve a binary system with stable helium layers, and consequently this is a topic that, although interesting, deserves further scrutiny. This is, however, beyond the scope of this paper. Another point of concern is how the resolution (that is, the number of SPH particles) affects the peak temperature. This has been investigated in several works — see, for instance, the discussions about this issue in Aznar-Siguán et al. (2013), and references therein. It is typically found that the peak temperatures may differ by a factor of 2 when low- and high-resolution simulations are compared, but these temperatures do not show an excessive dependence on the adopted resolution when the number of SPH particles is larger than $\sim 10^5$ — typically the differences amount to $\sim 15\%$.

We emphasize that when $q_{\mathrm{disk}} = 0.12$ is adopted — that is, for those mergers for which the eccentricity is high — the successive mass transfer episodes only happen when both stars are very close. Actually, it turns out that when both stars are at closest approach the secondary white dwarf is substantially tidally deformed, and the mass transfer episode occurs just after the passage through the periastron. However, soon after this, tidal deformations become smaller, so the mass transfer episode stops, and both components of the binary system recover their initial spherical symmetry for the rest of the orbit. On the contrary, when $q_{\mathrm{disk}} = 0.10$ is employed — corresponding to mergers driven by the emission of gravitational waves — the orbits are almost circular, and although the mass transfer episodes take place also at periastron, when the secondary is significantly distorted by tidal forces, the secondary star remains tidally deformed for the entire orbit, and thus the merger process proceeds in a smoother way.

In all four cases the successive mass transfer episodes modify the mass ratio of both components of the binary sys-

tem, and this in turn changes the respective orbits. Fig. 4 displays the trajectories of the center of mass of both components of the binary system. The left panels of this figure depict the trajectories of the centers of mass of the white dwarf components. The blue lines correspond to the cases in which the core of the AGB star is cold (labelled as CC), while the red ones show the cases in which we adopt a high temperature for the core of the AGB star (labelled as HC). In the right panels the trajectories of the center of mass of the AGB cores are displayed, using the same color coding. The top panels of this figure display the case in which $q_{\mathrm{disk}} = 0.12$. As can be seen, in this case the orbits are eccentric, while in the bottom panels, corresponding to $q_{\mathrm{disk}} = 0.10$, the orbits are initially nearly circular. As mentioned earlier, for both cases it turns out that during the first periastron passage the white dwarf transfers mass to the heavier AGB core and its radius increases. This radius increase starts a series of successive mass transfer episodes that ultimately lead to a merger.

We stress that the number of mass transfer episodes depends not only on the physical characteristics of the binary system but also on the number of SPH particles employed in the simulations, that is, on the spatial resolution. Although our resolution is enough for studying the overall properties of the dynamical interaction and the gross properties of the merged remnants, it is clear as well that our simulations provide only a lower limit to the number of mass transfer episodes. For this reason we do not quote the number of mass transfer episodes. Note as well that for the case in which $q_{\mathrm{disk}} = 0.10$ it is quite apparent that the last orbits are not circular, but instead during the final stages of the merger the orbit becomes quite eccentric. This final infall phase also takes place in the case of eccentric mergers. However, due to the difference of scales of the axis, it cannot
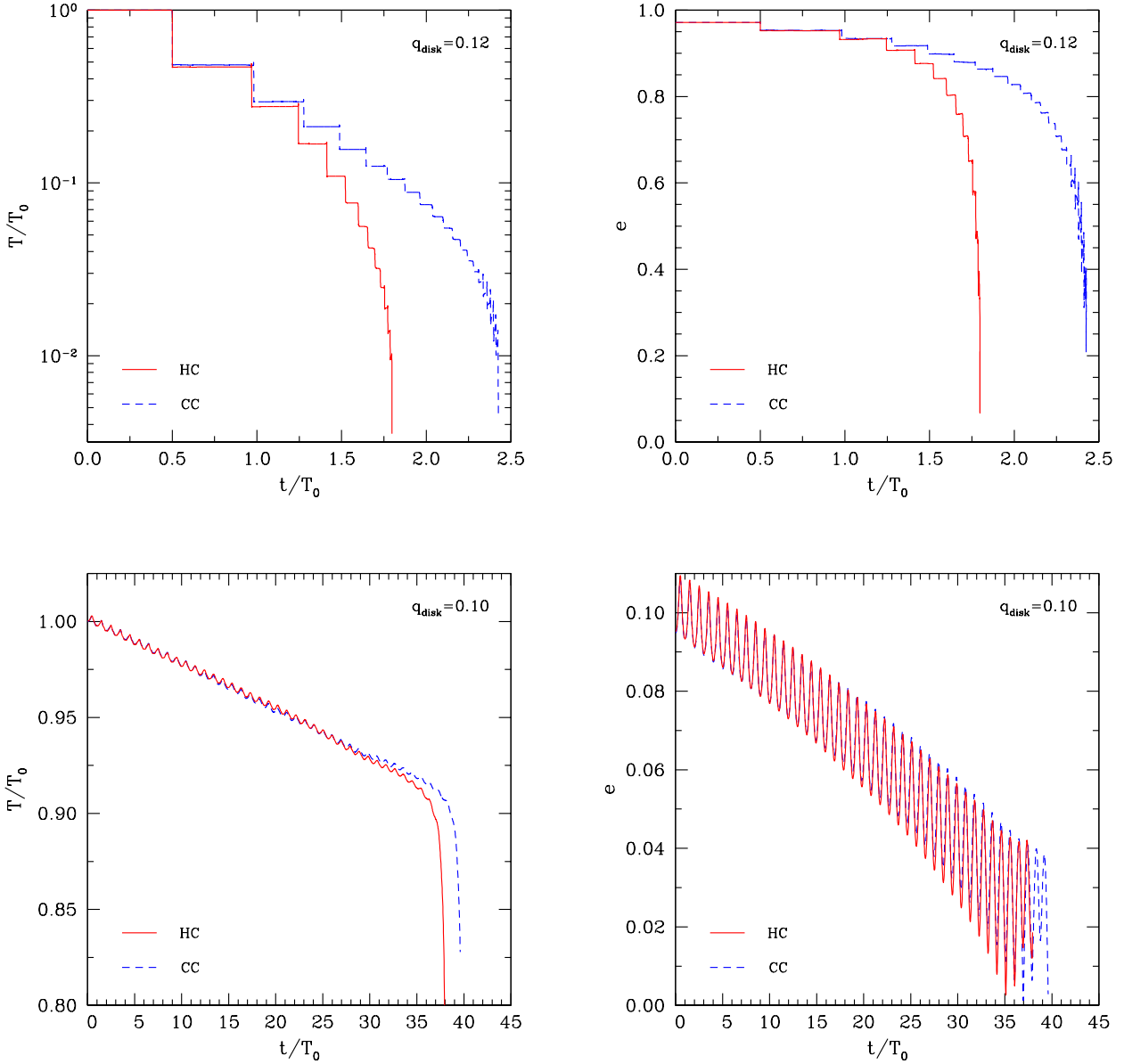
Figure 6. The evolution of the periods (left panels) and of the eccentricities (right panels) during the merger process. The top panels represent the case in which $q_{\rm disk} = 0.12$ is considered, and the bottom ones those in which $q_{\rm disk} = 0.10$ is adopted.

be well seen in the top panels of Fig. 4. Finally, it is also worth noting that the trajectories of the centers of mass for the case in which cold AGB cores are considered are only slightly different of those obtained in the case of hot AGB cores. Hence, the effects of the temperature of the AGB core on the overall dynamical evolution are very minor.

Figure 5 shows the mass accreted by the core of the AGB star ($M_{\rm acc}$), in units of the initial white dwarf mass ($M_{\rm WD}$), as a function of time in units of the initial period of the binary system, T_0. As in Fig. 4, the blue lines correspond to the case in which a cold merger is considered, while the red ones show the evolution for the hot merger. Again, the left panel displays the evolution for $q_{\rm disk} = 0.12$, whereas the right panel shows the same for $q_{\rm disk} = 0.10$. The mass

accreted by the core of the AGB star corresponds to the total mass of those SPH particles originally belonging to the disrupted secondary for which the gravitational attraction of the core of the AGB star is larger than that of the white dwarf.

Inspecting Fig. 5 we find that the mass accreted during the first mass transfer episode does not depend on the temperature of the AGB core, but depends critically on the adopted eccentricity. It is also interesting to point out that for the case in which a hot AGB core is adopted, mass is transferred faster than during the first mass transfer episode in successive passages through the periastron, for both $q_{\rm disk} = 0.12$ and 0.10. This is more noticeable for $q_{\rm disk} = 0.12$ — i.e., a merger in which the eccentricity is high.
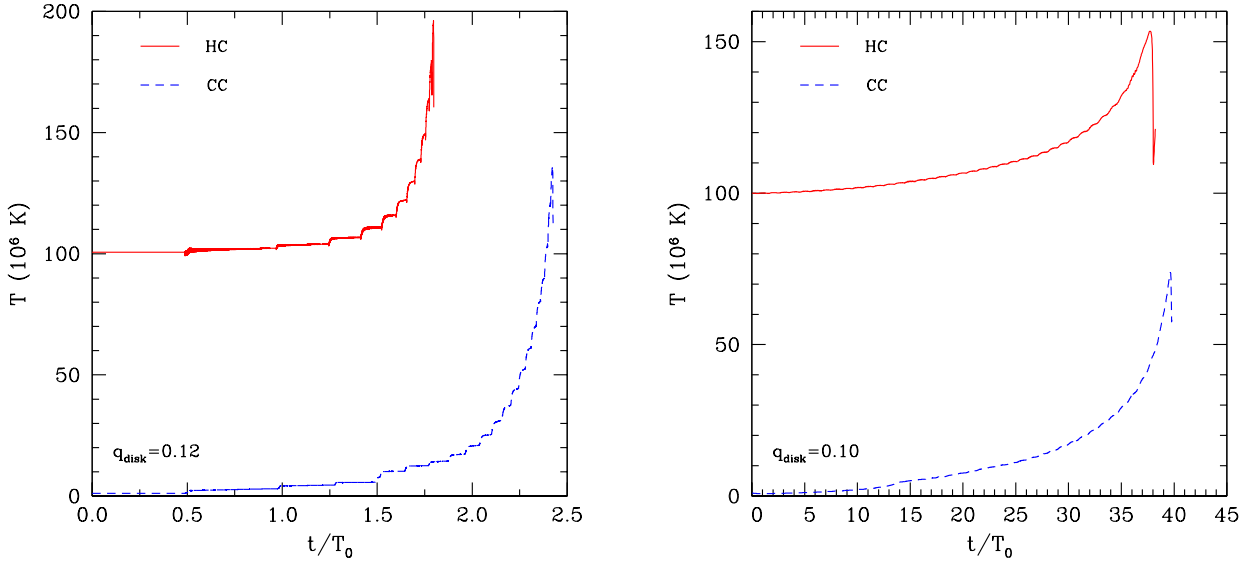
Figure 7. Average temperature of the core of the AGB star during the merger, for the case in which $q_{\rm disk} = 0.12$ is considered (left panel), and for that in which $q_{\rm disk} = 0.10$ (right panel).

Also, it is important to realize that for the cases in which a hot AGB core is adopted the amount of mass transferred in each one of the episodes is always larger than for the cases in which a cold AGB core is considered. All this stems from the fact that for a hot AGB core the degeneracy of the material of the outer layers is smaller than that of a cold core, and thus the core of the AGB star can accommodate more accreted mass.

In all the four cases studied here the mass transferred during the second mass transfer episode is larger than that transferred during the first periastron passage. This is a consequence of the substantial change of the orbital period after the first periastron passage, especially for $q_{\rm disk} = 0.12$. Specifically, for this case the period decreases by $\approx 50\%$ as seen in Fig. 6. This is less evident for the case in which $q_{\rm disk} = 0.10$ is adopted because in this case the period decreases by a modest $\approx 0.2\%$. All this translates into a smoother evolution, also for the successive mass transfer episodes, for the $q_{\rm disk} = 0.10$ cases. Thus, it turns out that the duration of the mergers is shorter for the cases in which a hot AGB is adopted, this feature being more pronounced for the case in which eccentric orbits are considered. Finally, note as well that in each accretion episode there is a small decline in the accreted mass. These declines correspond to matter, that although being initially accreted by the core of the AGB star, is bounced back to the debris region shortly after.

To better illustrate the dynamical evolution of the mergers Fig. 6 displays the evolution of the periods (left panels) and eccentricities (right panels) of the binary systems studied here. As before, the top panels depict the evolution of the orbital parameters for $q_{\rm disk} = 0.12$, whilst the bottom ones show that for the case in which $q_{\rm disk} = 0.10$ is adopted. As can be clearly seen, in all four simulations after each mass transfer episode the periods of the binary

systems decrease and the orbits become circularized. These general trends become more accentuated as the evolution proceeds. Although for $q_{\rm disk} = 0.10$ initially the period decreases smoothly in an almost linearly way with a shallow slope, after $t \sim 35 T_0$ the white dwarf almost plunges on top of the core of the AGB star. This is in contrast with what occurs for $q_{\rm disk} = 0.12$, for which the decrease in the orbital periods occurs faster during the initial stages of the dynamical evolution, in marked steps, and the white dwarf merges with the core of the AGB star in very few orbital periods, $\sim 2 T_0$. The right panels of this figure show that the eccentricity also decreases for increasing times. For $q_{\rm disk} = 0.12$ this occurs in marked steps, as it occurs with the orbital periods, a consequence of the succesive passages through the periastron, while for $q_{\rm disk} = 0.10$ the eccentricity also decreases but oscillates arroung a mean (decreasing) value. This is caused by tidal forces.

Figure 7 shows the average temperature of the core for the different cases considered here. To compute this temperature we averaged the temperature of those particles which were originally used to model the core, and thus we did not take into account the accreted material from the disrupted white dwarf. This is an important detail, since the maximum temperatures during the evolution of the simulated cases of coalescence are not reached in the core of the merged remnant but in the hot corona formed during the interaction — see below. As before, the left panel and right panels represent, respectively, the cases for which $q_{\rm disk} = 0.12$ and $q_{\rm disk} = 0.10$ are adopted. As can be seen, since for eccentric orbits the amount of mass transferred during each dynamical episode is larger, the temperatures are increased more noticeably. Actually, the temperature is not raised homogenously in the entire core. Specifically, the temperature of the outer layers of the core is notably increased after every mass transfer episode, while the temperature of the very deep in-

Table 1. Some relevant characteristics of the merged remnants. By columns: (1) value of q_{disk} from equation 1, (2) type of run, hot (HC) or cold (CC) core of the AGB star, (3) maximum temperature attained during the dynamical interaction, (4) nuclear energy released, (5) duration of the merger, (6) Mass of the merged remnant at the end of the simulations, (7) mass of Keplerian disk at the end of the simulations, (8) mas of the extended shroud at the end of the simulations, (9) mass of fall-back material, (10) ejected mass, (11) maximum temperature of the merged remnant, (12) maximaum angular speed of the hot corona at the end of the simulations.

q_{disk}	Run	T_{peak} (K)	E_{nuc} (erg)	Δt (s)	M_{mr} ($M_\odot$)	M_{disk} ($M_\odot$)	M_{shroud} ($M_\odot$)	M_{fb} ($M_\odot$)	M_{ej} ($M_\odot$)	T_{max} (K)	ω_{max} (s^{-1})
0.12	HC	9.23×10^8	1.13×10^{39}	18343	0.88	0.36	9.08×10^{-2}	2.19×10^{-2}	1.74×10^{-2}	3.56×10^8	0.23
	CC	8.55×10^8	3.54×10^{37}	24784	0.88	0.35	9.84×10^{-2}	2.02×10^{-2}	1.80×10^{-2}	3.53×10^8	0.25
0.10	HC	8.74×10^8	1.12×10^{39}	2599	0.93	0.39	4.86×10^{-2}	2.43×10^{-3}	7.37×10^{-4}	2.97×10^8	0.30
	CC	8.18×10^8	4.77×10^{37}	2710	0.91	0.41	4.59×10^{-2}	2.56×10^{-3}	8.70×10^{-4}	3.10×10^8	0.32

terior of the core remains nearly constant. As it should be expected, the final temperatures of the hot cores are much larger than their cold counterparts.

Table 1 shows some relevant characteristics of the stellar interactions studied in this paper. In columns three to five of this table we list, respectively, the maximum temperature reached during the dynamical interaction, T_{peak}, the total nuclear energy released, E_{nuc}, and the total duration of the merger, Δt. The maximum temperature always is reached at the base of the accreted layer. The nuclear energy is essentially released by carbon burning reactions and the α chains. Note that the nuclear energy released in those mergers in which the core of the AGB is hot is typically 25 times larger than that released when cold cores are involved. The reason for this is that for mergers involving hot AGB cores nuclear reactions occur in a region which is significantly larger than that in which cold cores are considered. Most of the nuclear reactions occur on top of the almost rigid surface of the core of the AGB star, as the material of the disrupted white dwarf is accreted, compressed and heated. A discussion of the details of the distribution of the chemical composition in the remnant is out of the scope of this paper, and will be presented elsewhere. However, we mention here that these results are in line with our previous simulations of merging and colliding white dwarfs (Lorén-Aguilar, Isern & García-Berro 2009, 2010; Aznar-Siguán et al. 2013, 2014), which in turn agree with the calculations of Raskin et al. (2014) and Dan et al. (2014).

Again, we emphasize that the duration of the merger not only depends on the physical characteristics of the coalescing stars, but also on the adopted resolution. The reason for this is that, as it occurs with DD mergers, the durations of the mass transfer episodes depend on the extent to which the outer layers of the donor star can be resolved. In most practical situations the particle masses are such that the resolvable mass transfer rate is already a substantial fraction of the total system mass — see Dan et al. (2011) for a detailed discussion of this issue. Hence, these durations should be regarded as indicative, and can be only used to compare the different cases studied here, which were computed with the same spatial resolution and input physics.

Figs. 2, 3 and 5 reveal that the peak temperature is reached at $t = 1.8T_0$ and $t = 2.4T_0$ for the hot and cold cores of the AGB star when $q_{disk} = 0.12$ and at $t = 38.1T_0$

and $t = 40.3T_0$ for the case in which $q_{disk} = 0.10$. When this occurs the fraction of the secondary white dwarf that has been accreted onto the core of the AGB star is $\gtrsim 20\%$ for $q_{disk} = 0.12$, whereas for $q_{disk} = 0.10$ it is $\lesssim 10\%$. All this has a direct effect on the thermonuclear reaction rates, and consequently on the total nuclear energy released during the interactions. In particular, while for the case of hot cores the total nuclear energy released is $\approx 10^{39}$ erg, for the cold ones it is much smaller, $\approx 10^{37}$ erg. The nuclear energy released is similar for the eccentric orbits and the non-eccentric ones for a fixed temperature of the AGB core, despite the difference in the peak temperatures achieved during the interaction.

Finally, we note that eccentric orbits ($q_{disk} = 0.12$) result in mergers with durations of a few hours, much longer than those of mergers with $q_{disk} = 0.10$, for which the durations are smaller than ~ 1 hour. However, we remind that for the case of eccentric orbits the coalescence occurs in just a couple of initial orbital periods, while for circular ones the merger lasts for several initial orbital periods.

4.2 The remnants of the interaction

In this section we analyze with the help of Figs. 8, 9, 10 and Table 1 the structure of the remnants of the interaction. The general appearance of the remnants resulting from the interaction is similar for all the cases studied in this paper, and moreover is similar to that found in previous simulations of the DD scenario for similar masses — see, for instance, Lorén-Aguilar, Isern & García-Berro (2009), and references therein. The remnants of the interactions when simulations were stopped consist of a central degenerate object which contains all the mass of the core of the AGB star and some accreted mass. This central object spins as a rigid body and its angular momentum arises from the conversion of the orbital angular momentum of the binary system to rotational one. This core is surrounded by a corona, which contains a sizable fraction, $\sim 18\%$ for eccentric mergers and $\approx 27\%$ for circular ones, of the mass of the disrupted secondary (the white dwarf). The material of the corona is hot — a consequence of the material of the disrupted secondary being compressed on top of the almost rigid surface of the core of the AGB star — and rotates differentially — a consequence of the several mass transfer episodes occurring in the dynamical interaction. Most of the material of the secondary
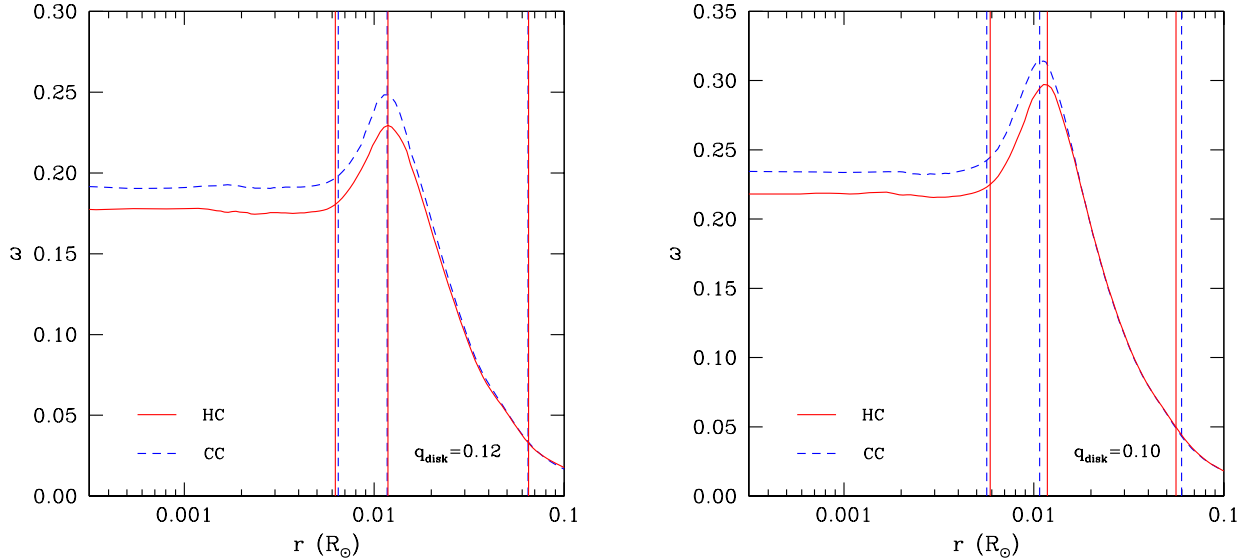
Figure 8. Rotational velocity profiles as a function of the spherical radius in solar units, at times $t/T_0 = 1.8115$ and 2.4476 for the hot (solid red lines) and cold (dashed blue lines) AGB cores of the simulation in which $q_{disk} = 0.12$, and $t/T_0 = 40.2378$ and 41.9690 for the case in which $q_{disk} = 0.10$ is adopted, respectively. These times correspond to our last computed models. In the left panel we represent the profiles for $q_{disk} = 0.12$, while the right one corresponds to $q_{disk} = 0.10$. Note that for large distances the spherical radius is not a valid representation of the merged configuration, as the assumption of spherical symmetry is only fulfilled to a good approximation in the innermost regions of the merged remnant. The leftmost solid vertical lines show the outer boundaries of the respective degenerate remnants. The middle vertical lines show the location of the outer edges of the corresponding coronae. The rightmost vertical lines mark the outer edges of the respective Keplerian disks.

($\sim 82\%$ and $\approx 73\%$, respectively, for eccentric and circular mergers) that is not accreted on the central object goes to form a thick accretion disk, with a Keplerian velocity profile. Additionally, there is an extended shroud made of particles that have orbits with large inclinations with respect to the orbital plane. Also, some SPH particles have highly eccentric orbits and will ultimately fall back onto the primary. Finally, we find that very little mass is ejected from the system. All these regions are clearly shown in Fig. 8, where we plot the angular velocity of the remnant as a function of the spherical radius for the remnants of the interactions studied here. The vertical lines show from left to right, respectively, the locations of the outer edge of the remnant, of the hot, rapidly rotating corona and of the Keplerian disk.

Table 1 lists also some of the characteristics of the merged remnant. In column 6 we list the mass of the central merged object (M_{mr}) — that is, the sum of the mass of the undisturbed AGB core and of the hot corona — while in column 7 the mass of the Keplerian disk (M_{disk}) is listed. The precise location of the inner edge of the hot corona is defined as the (spherical) mass coordinate for which the angular velocity is no longer constant, while the outer boundary of this region is defined as the point where the profile of angular velocities of the remnants is the Keplerian. In this table we also show the mass of the extended shroud (M_{shroud}), that of the fallback material (M_{fb}), as well as the mass ejected from the system (M_{ej}) — columns 8, 9 and 10, respectively. As mentioned, the shroud is composed of material coming from the disrupted secondary that has approximately a spherical distribution. The fallback material is composed of particles

belonging to the debris region that have very eccentric orbits as a result of the extreme conditions found during the very first stages of the dynamical interaction, but are still gravitationally bound to the merged remnant. Thus, it is expected that this material will ultimately fall back onto the central remnant at some later time (Rosswog 2007). To compute the amount of mass in the debris region that will eventually fall back on the central object we followed the same procedure described in Aznar-Siguán et al. (2014). Note that there is as well some material that is not gravitationally bound to the remnant and might escape, but the merger episodes are essentially conservative. We would like to remark that we do not look for a possible formation of jets and disk winds which, in the DD scenario influece the appearance of an explosion if it occurs shortly after the merger (Levanon, Soker & García-Berro 2015). Finally, for the sake of completeness we also list the maximum temperature (T_{max}) and the maximum angular velocities (ω_{max}) of the hot corona, columns 11 and 12, respectively.

4.2.1   The central compact object

As can be seen in Table 1, the angular velocities of the remnants do not depend appreciably on the adopted temperature of the core of the AGB star, although there are significant differences depending on the value of q_{disk}. The reason for this is that in the coalescence studied here the rigid rotation of the core of the AGB star arises from the conservation of angular momentum. That is, the orbital angular momentum of the pair is basically invested in spinning
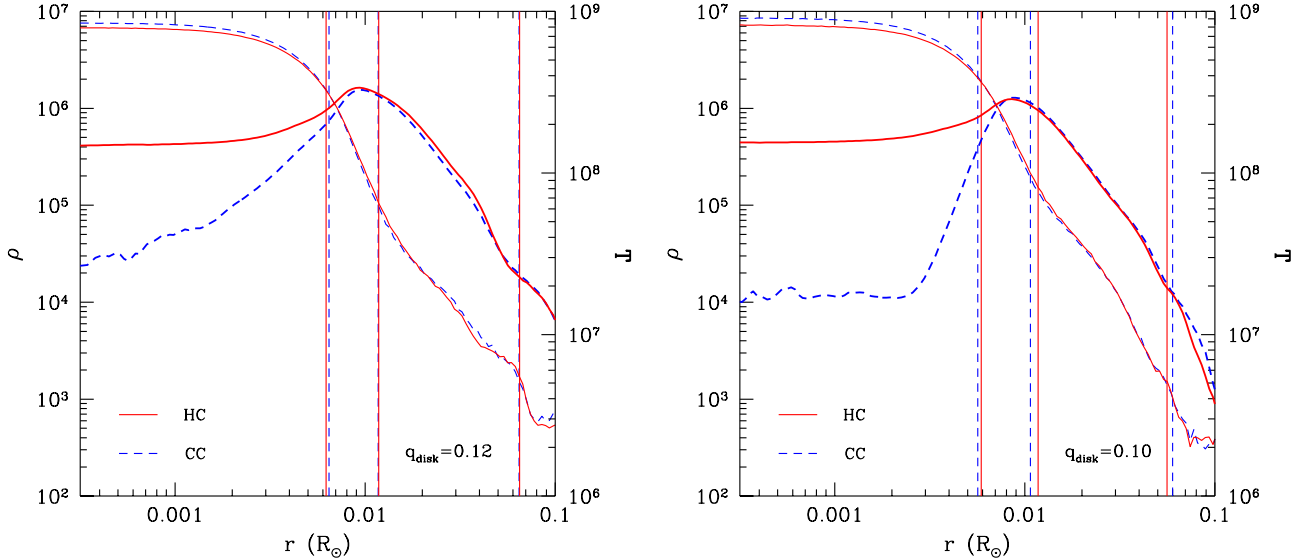
Figure 9. Density (thin lines) and temperature (thick lines) profiles of the central part of the remnants, at the same times shown in Fig. 8. The left panel shows the profiles of the hot (solid red lines) and cold (dashed blue lines) AGB cores of the simulation in which $q_{disk} = 0.12$, while the right panel shows the same quantities for $q_{disk} = 0.10$. As before, the abscissa is the spherical radius in solar units, and the vertical lines show the same locations explained in Fig. 8.

up the primary and the previously described corona, and to form the Keplerian disk. Nevertheless, the angular velocity of the remnants of the mergers in which a cold AGB core is involved are somewhat larger in both cases. This is due to the slightly smaller radii of these configurations (see Fig. 9 below), which in turn is a consequence of their larger degeneracies.

We now compare the angular velocities obtained for different values of q_{disk}. As shown in Table 1, when $q_{disk} = 0.10$ is adopted the angular velocities are larger. In particular, we find that for this case the inner regions of the merged remnant rotate uniformly at a speed $\omega \simeq 0.22$ s^{-1}, whereas in the corona a maximum angular velocity of $\omega_{max} \simeq 0.31$ s^{-1} is reached. For the case in which $q_{disk} = 0.12$ these angular velocities are, respectively, $\omega \simeq 0.18$ s^{-1}, and $\omega_{max} \simeq 0.24$ s^{-1}, somewhat smaller than those of the case in which $q_{disk} = 0.10$ is employed. The orbital angular momentum of the binary systems studied here is $J = 5.96 \times 10^{50}$ erg s for $q_{disk} = 0.12$, and $J = 4.63 \times 10^{50}$ erg s when $q_{disk} = 0.10$. Since the merger is almost conservative (very few particles acquire energies large enough to escape from the merged remnant) this angular momentum is distributed essentially in spinning up the core of the AGB star, in the differential rotation of the hot corona and in Keplerian disk.

For a hot merger their respective angular momenta are $J_{core} \simeq 1.4 \times 10^{49}$ erg s, $J_{corona} \simeq 4.4 \times 10^{49}$ erg s and $J_{disk} \simeq 2.8 \times 10^{50}$ erg s for $q_{disk} = 0.12$, and $J_{core} \simeq 1.5 \times 10^{49}$ erg s, $J_{corona} \simeq 6.7 \times 10^{49}$ erg s and $J_{disk} \simeq 3.2 \times 10^{50}$ erg s for $q_{disk} = 0.10$, respectively. For the case of a cold merger these values do not differ much. Hence, the orbital angular momentum of the eccentric merger is larger than that of the circular one, and moreover the angular momenta are distributed in a different way in both cases. Specifically, the

angular momentum of the corona for $q_{disk} = 0.12$ is noticeably smaller than that of the merger in which $q_{disk} = 0.10$ is adopted, but the mass of their respective coronae do not differ that much. Also the angular momentum of the newly formed disk of the eccentric merger is significantly smaller than that of the circular one. Consequently, more angular momentum is stored in these (outer) regions for the case in which $q_{disk} = 0.10$ is adopted when compared to the case in which $q_{disk} = 0.12$. Finally, for the the simulations in which $q_{disk} = 0.12$ is employed the ejected mass is considerably larger than that of the case in which $q_{disk} = 0.10$ is used. This mass carries some angular momentum. All this explains why the merged remnant spins at a slower rate for $q_{disk} = 0.12$. All this is a consequence of the dynamical evolution during the merger. We remind that for $q_{disk} = 0.12$ the evolution proceeds in abrupt steps, while for $q_{disk} = 0.10$ mass is accreted in a more gentle way.

Figure 9 shows the density (dashed lines) and temperature (solid lines) profiles, for the case in which $q_{disk} = 0.12$ (left panel) and the for the case in which $q_{disk} = 0.10$ (right panel). The maximum temperature (T_{max}) in all the remnants is very similar, close to 3×10^8 K, being slightly higher for the remnants of the eccentric mergers. This can be easily understood in terms of the evolution during the last merger episode. In particular, it has been already mentioned that for eccentric mergers the mass transfer episodes are more dramatic than for the case of nearly circular orbits. Hence, the matter of the disrupted secondary white dwarf acquires larger accelerations and, consequently, is compressed more violently on the surface of the primary star. Thus, the temperatures of the external layers of the merged configuration are larger, and a hotter corona is obtained.

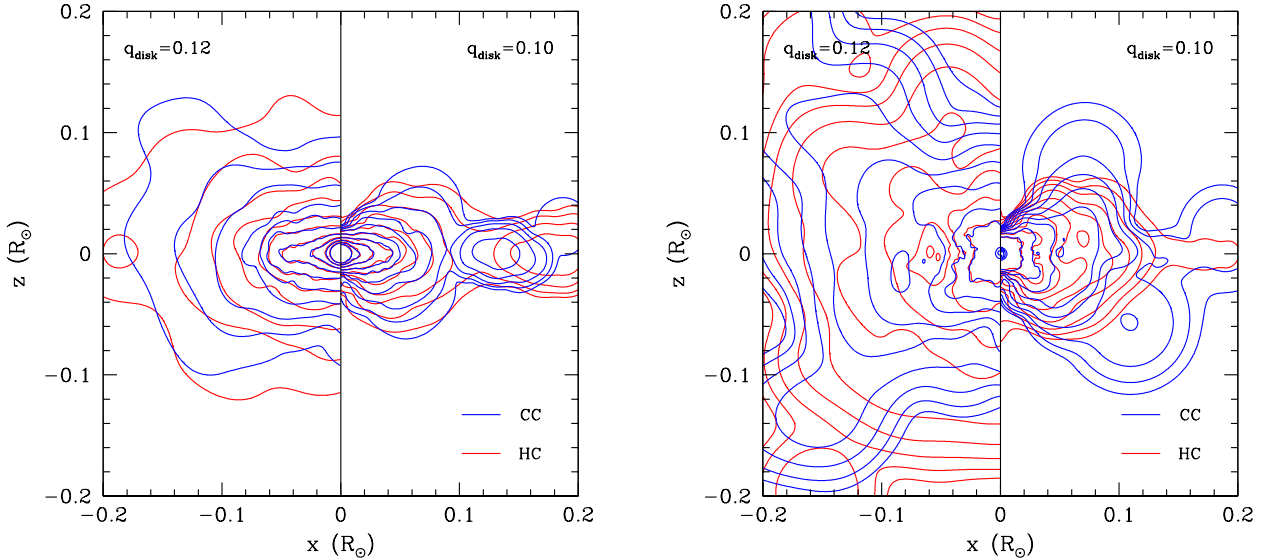The stronger interaction of the accreted matter with the

Figure 10. Left panel: density contour lines of the remnants across the meridional plane. Right panel: temperature contour lines across the same section. These density and temperature maps correspond to our last computed models, and the evolutionary times are the same of Fig. 9. The remnants represented with negative x coordinates correspond to the case in which $q_{\rm disk} = 0.12$, while for positive values of x the case in which $q_{\rm disk} = 0.10$ is represented. For both cases the outermost contour of the density profile corresponds to a density of 1 g cm^{-3} and the successive contours increase logarithmically inwards in constant steps of $\log \rho = 0.62$. The contour of maximum density corresponds to $\sim 3.8 \times 10^5$ g cm^{-3}. For the temperature the outermost contour corresponds to $\sim 3 \times 10^5$ K and the successive contours increase inwards logarithmically in steps of $\log T = 0.33$. The maximum temperature contour corresponds to $\sim 1.4 \times 10^8$ K. This temperature is reached in the hot corona, while the innermost regions of the merged remnant in the case of a core with small temperature merger are colder — see Fig. 7. See the online edition of the journal for a color version of this figure.

primary during the successive mass transfer episodes leaves also clear imprints on the structure of the internal regions of the merged remnant. Specifically, for the case of eccentric mergers in which a cold core of the AGB star is considered, the temperature of the outermost regions of the initially isothermal core begins to increase at earlier times during the coalescence, when compared to those in which a circular orbit is involved. Consequently, by the end of the merger process the core of this remnant is no longer isothermal. On the contrary, the core in the case of a circular orbit remains nearly isothermal — see Fig. 9. Finally, owing to the substantial degeneracy of the material of the core of the AGB star, the density profiles obtained in all the four simulations presented here are very similar.

4.2.2 The debris region

It has been already discussed that the temperature of the AGB core barely plays a role in the dynamical evolution of the merger process, and in determining the structure of the merged remnant. Instead, the most important parameter is the eccentricity of the initial orbits of both components of the binary system. This is true as well for the debris region formed around the merged remnants. The masses of the fallback and of the ejected material are, respectively, $M_{\rm fb} \simeq 2.1 \times 10^{-2}\, M_\odot$ and $M_{\rm ej} \simeq 1.8 \times 10^{-2}\, M_\odot$ for eccentric mergers, while for circular orbits the masses are much smaller, $M_{\rm fb} \simeq 2.5 \times 10^{-3}\, M_\odot$ and $M_{\rm ej} \simeq 8.1 \times 10^{-4}\, M_\odot$. The larger fallback and ejected masses in the case of eccen-

tric mergers are a consequence of the longer durations (or, equivalently, larger orbital separations) of the mass transfer episodes — see Figs. 5 and 6.

As well, the masses of the respective shrouds are relatively different, $M_{\rm shroud} \simeq 9.2 \times 10^{-2}\, M_\odot$ for $q_{\rm disk} = 0.12$ and $M_{\rm shroud} \simeq 4.7 \times 10^{-2}\, M_\odot$ for $q_{\rm disk} = 0.10$. This is again a consequence of the very different number of mass transfer episodes occurring in both simulations. Actually, for $q_{\rm disk} = 0.12$ we find that some mass of the disrupted white dwarf flows around the region located in the opposite direction of the line connecting both stars of the system, and acquires high velocities when colliding with the primary star, forming this extended shroud. The size of this extended region does not depend much on the temperature adopted for the core of the AGB star. This can be seen in Fig. 10, where the density (left panel) and temperature (right panel) contours of the merged remnant in the meridional plane are displayed. In this figure the sub-panel with negative values of the x-coordinate corresponds to the case $q_{\rm disk} = 0.12$, whereas that with positive values shows the same contours for the case in which $q_{\rm disk} = 0.10$ is adopted.

As can be seen in Fig. 10, both the density and the temperature decrease as the distance to the central compact object increases, independently if we consider the remnants of eccentric or circular mergers. However the decline rate of both the density and the temperature for eccentric mergers is smaller than for circular orbits, resulting in a more extended debris region, which moreover is hotter. Additionally, the density and temperature profiles also have a different

behavior near the polar regions of the central remnant. For mergers arising from circular orbits there is a region near the z-axis (the vertical axis in this figure) where the density and the temperature contour lines converge towards the poles, in contrast with what happens for the case of eccentric mergers, for which this region is absent, and the contour lines are perpendicular to this axis. These differences between both profiles are a consequence of how the material of the disrupted secondary white dwarf is distributed on top of the primary (the core of the AGB star) during the dynamical interaction.

The final infall of the disrupted secondary onto the unaltered primary for $q_{\rm disk} = 0.10$ seen in Figs. 3 and 4, does not allow matter to be redistributed on the primary, but instead concentrates it in the orbital plane. Besides, the circular density contours that appear at the right of the remnant correspond to a spiral arm of matter infalling to the primary. Since SPH codes are not able to follow properly angular momentum transport, we stopped the simulations at a reasonable time after the complete disruption of the secondary. In particular, for $q_{\rm disk} = 0.12$ we stopped the simulations at $t/T_0 = 1.8115$ and $t/T_0 = 2.4476$ for the hot and cold merger, respectively. For $q_{\rm disk} = 0.10$ these times are, respectively, $t/T_0 = 40.2378$ and $t/T_0 = 41.9690$. In this case, the secondary had no time to be totally distributed over the primary and the spiral arm formed during the infalling phase is still present. The more flat structure for $q_{\rm disk} = 0.10$, which is more similar to that usually found in the simulations of the DD scenario, might lead to jets and disk winds that might alter the observations if explosion occurs shortly after merger (Levanon, Soker & García-Berro 2015). Finally, the outer edges of the Keplerian disks formed during the merger process are located where the density distribution in the equatorial plane has no longer axial symmetry. In all cases this occurs at $\sim 0.06\,R_\odot$.

5 SUMMARY AND CONCLUSIONS

In this paper we have simulated the coalescence of a white dwarf with the core of a massive AGB star, in the context of the so-called core-degenerate scenario for SNe Ia. Specifically, we have computed the merger of an otherwise typical white dwarf of mass $0.6\,M_\odot$ with the core of an AGB star of mass $0.77\,M_\odot$, which is a typical case (Kashi & Soker 2011). This has been done for two temperatures of the AGB core, $T = 10^6$ K and 10^8 K, and for two assumptions about the mass of the disk formed during the common envelope phase. In particular, we have studied a first case in which the mass of the disk is $M_{\rm disk} = 0.12(M_{\rm core} + M_{\rm WD})$, which corresponds to the critical mass ratio for which a merger is guaranteed as a consequence of the interaction with the disk formed during the common envelope phase. The second case studied here corresponds to a binary system surviving the common envelope phase with a mass ratio 0.10, which is below the critical one, and for which the merger is driven by the emission of gravitational waves. The first of these cases results in a pair with a highly eccentric orbit, whereas for the second one the orbits of the members of the binary system are circular, and similar to those expected for the DD scenario for SNe Ia.

Our SPH simulations show that temperature of the core of the AGB star has little influence on the overall dynamical evolution of the merging process and on the characteristics of the merger remnant, but the initial eccentricity of the binary system has a large impact on both the dynamical evolution of the merger and on the properties of the merged object. In particular, in both cases the white dwarf is totally disrupted in a series of mass transfer episodes, which occur at closest approach. However, the duration of the coalescence is notably different in both cases. Specifically, we found that for the case of an eccentric merger the disruption of the secondary white dwarf occurs in very few orbital periods, whereas for the case of the mergers in which circular orbits are adopted this process lasts for many orbital periods. Nevertheless, the initial orbital periods in both cases are very different — 10,126 s and 65 s, respectively — so the total time required to disrupt the secondary white dwarf turns out to be larger for the case of eccentric orbits.

In all the four cases studied in this paper the coalescence process is almost conservative, and little mass is ejected from the system, $\sim 2 \times 10^{-2}\,M_\odot$ at most. Nevertheless, eccentric mergers eject ~ 25 times more mass than that ejected by binary systems with circular orbits. The peak temperatures achieved during the merging process are rather high, of the order of 8×10^8 K, but not enough to power a prompt detonation upon merger. As for the final temperature of the merger remnant it is interesting to realize that for the cases studied here the temperature profile peaks off-center. The possibility that carbon is ignited in the remnant, thus producing a rapidly spinning oxygen-neon white dwarf, has been discussed by Saio & Nomoto (2004), Yoon & Langer (2004), and Yoon & Langer (2005). Our results do not support a prompt off-center ignition, since the peak temperature obtained at the end of our simulations is too low, and moreover the temperature peaks in a region where the densities are relatively small. However, even though carbon in our models is not ignited immediately during the merger process, it may occur at later times, when the high entropy material begins to cool and compress the material near the temperature peak. Nevertheless, this depends on the not yet well known viscous timescale of the disk, which characterizes the transport of disk mass inwards and angular momentum outwards, and on the thermal timescale of the merger product. Thus, the post-merger evolution has received recently considerable interest (van Kerkwijk, Chang & Justham 2010; Schwab et al. 2012; Shen et al. 2012; García-Berro et al. 2012; Ji et al. 2013; Zhu et al. 2013; Beloborodov 2014) but a clear consensus on whether a powerful carbon ignition can develop at later times has not emerged yet.

The structure of the merged remnant consists of a central compact object containing all the mass of the core of the AGB star and some mass from the disrupted secondary star, which is surrounded by a hot, differentially rotating corona. This corona is made of about 18% of the mass of the disrupted white dwarf, for the case of eccentric mergers, and somewhat larger ($\sim 27\%$) for circular ones. Finally, surrounding this central compact object there is a heavy, rapidly-rotating Keplerian disk, and an extended shroud of material which are formed by the rest of the mass of the disrupted white dwarf that has approximately ellipsoidal shape. This configuration is essentially the same found for DD mergers. However, the structure of the debris region is different depending on the initial eccentricity of the merger.

For mergers with initially circular orbits the matter of the disrupted white dwarf concentrates in regions near the orbital plane, and little mass is found in the polar regions, whereas for eccentric mergers part of the mass of the disrupted white dwarf is distributed along the central compact object, and the merged configuration adopts an ellipsoidal shape. In the debris region there is also some fraction of SPH particles with highly eccentric orbits. This material will ultimately interact with matter in the Keplerian disk and will fall back onto the central compact remnant. The mass of this fallback material is typically or the order of $2 \times 10^{-2} M_\odot$ for the case of the binary systems with eccentric orbit, and ten times smaller for those with circular ones. In all cases, this central object rotates as a rigid body, with typical angular velocities ~ 0.18 s^{-1} for the case of eccentric mergers and ~ 0.22 s^{-1} for circular ones. These rotation velocities arise from the conversion of orbital angular momentum to rotational one, as it happens for DD mergers.

We would like to emphasize that if the disk, fallback material, and the material of the extended shroud are finally accreted, as it is commonly thought, the mass of the remnant would be $\approx 1.35 M_\odot$. If this is the case, after cooling and losing angular momentum this remnant might eventually explode. Of course, assessing such possibility requires modelling the viscous phase of the merger, which transports disk mass inwards and angular momentum outwards. This phase has typical timescales ranging from 10^3 s to 10^4 s, during which the disk might launch jets and winds (Levanon, Soker & García-Berro 2015), and it cannot be followed using SPH techniques. If, nonetheless, all this mass is accreted and the remnant explodes the delay would be very long, up to millions of years, or even longer (Ilkov & Soker 2012). In particular, for accretion of helium onto a carbon-oxygen white dwarf in a stable regime, in a recent study Piersanti, Tornambé & Yungelson (2014) found a delay of up to millions of years, in agreement with previous calculations of this kind (Nomoto & Iben 1985; Saio & Nomoto 2004; Yoon, Podsiadlowski & Rosswog 2007; Shen & Bildsten 2009). It remains to be checked if the same might occur for the CD merger process.

In summary, this first set of simulations of the CD scenario for SNe Ia demonstrates the need of exploring in more detail the effects of the eccentricity (and possibly of the temperature) on the overall dynamical evolution of the merger and on the properties of the merged configurations obtained in this scenario, especially when more massive stars are involved. The simulations presented here are a first important step in this direction. Future works will undoubtedly allow us to characterize and place tight constraints on the most salient features of this scenario, and may possibly help in quantifying the fraction of these mergers that contributes to the total SNe Ia rate, thus filling a gap and complementing what we already learned from the existing simulations of the DD scenario.

References

Artymowicz P., Clarke C. J., Lubow S. H., Pringle J. E., 1991, ApJ, 370, L35

Aznar-Siguán G., García-Berro E., Lorén-Aguilar P., José J., Isern J., 2013, MNRAS, 434, 2539

Aznar-Siguán G., García-Berro E., Magnien M., Lorén-Aguilar P., 2014, MNRAS, 443, 2372

Balsara D. S., 1995, J. Comp. Phys., 121, 357

Barnes J., Hut P., 1986, Nature, 324, 446

Beloborodov A. M., 2014, MNRAS, 438, 169

Benz W., Cameron A. G. W., Press W. H., Bowers R. L., 1990, ApJ, 348, 647

Bildsten L., Shen K. J., Weinberg N. N., Nelemans G., 2007, ApJ, 662, L95

Briggs G. P., Ferrario L., Tout C. A., Wickramasinghe D. T., Hurley J. R., 2015. MNRAS, in press

Chiosi E., Chiosi C., Trevisan P., Piovan L., Orio M., 2015, MNRAS, 448, 2100

Cyburt R. H. et al., 2010, ApJS, 189, 240

Dan M., Rosswog S., Brüggen M., Podsiadlowski P., 2014, MNRAS, 438, 14

Dan M., Rosswog S., Guillochon J., Ramirez-Ruiz E., 2011, ApJ, 737, 89

Eggleton P. P., 1983, ApJ, 268, 368

Foley R. J. et al., 2013, ApJ, 767, 57

García-Berro E. et al., 2012, ApJ, 749, 25

Guerrero J., García-Berro E., Isern J., 2004, A&A, 413, 257

Guillochon J., Dan M., Ramirez-Ruiz E., Rosswog S., 2010, ApJ, 709, L64

Han Z., Podsiadlowski P., 2004, MNRAS, 350, 1301

Hernquist L., Katz N., 1989, ApJS, 70, 419

Hillebrandt W., Kromer M., Röpke F. K., Ruiter A. J., 2013, Frontiers of Physics, 8, 116

Iben J. I., Tutukov A. V., 1984, ApJS, 54, 335

Ilkov M., Soker N., 2012, MNRAS, 419, 1695

Ilkov M., Soker N., 2013, MNRAS, 428, 579

Itoh N., Hayashi H., Nishikawa A., Kohyama Y., 1996, ApJS, 102, 411

Ji S. et al., 2013, ApJ, 773, 136

Jordan I. G. C., Perets H. B., Fisher R. T., van Rossum D. R., 2012, ApJ, 761, L23

Kashi A., Soker N., 2011, MNRAS, 417, 1466

Kushnir D., Katz B., Dong S., Livne E., Fernández R., 2013, ApJ, 778, L37

Levanon N., Soker N., García-Berro E., 2015, MNRAS, 447, 2803

Livio M., Riess A. G., 2003, ApJ, 594, L93

Lorén-Aguilar P., Isern J., García-Berro E., 2009, A&A, 500, 1193

Lorén-Aguilar P., Isern J., García-Berro E., 2010, MNRAS, 406, 2749

Maoz D., Mannucci F., Nelemans G., 2014, ARA&A, 52, 107

Meng X., Yang W., 2012, A&A, 543, A137

Monaghan J. J., 1997, Journal of Computational Physics, 136, 298

Monaghan J. J., Lattanzio J. C., 1985, A&A, 149, 135

Moore K., Townsley D. M., Bildsten L., 2013, ApJ, 776, 97

Morris J. P., Monaghan J. J., 1997, Journal of Computational Physics, 136, 41

Nomoto K., 1982, ApJ, 253, 798

Nomoto K., Iben, Jr. I., 1985, ApJ, 297, 531

Pakmor R., Kromer M., Röpke F. K., Sim S. A., Ruiter A. J., Hillebrandt W., 2010, Nature, 463, 61

Pakmor R., Kromer M., Taubenberger S., Springel V., 2013, ApJ, 770, L8

Perets H. B. et al., 2010, Nature, 465, 322

Piersanti L., Tornambé A., Yungelson L. R., 2014, MN-RAS, 445, 3239

Price D. J., 2007, PASA, 24, 159

Price D. J., Monaghan J. J., 2007, MNRAS, 374, 1347

Raskin C., Kasen D., Moll R., Schwab J., Woosley S., 2014, ApJ, 788, 75

Raskin C., Timmes F. X., Scannapieco E., Diehl S., Fryer C., 2009, MNRAS, 399, L156

Rosswog S., 2007, MNRAS, 376, L48

Rosswog S., Kasen D., Guillochon J., Ramirez-Ruiz E., 2009, ApJ, 705, L128

Ruiter A. J., Belczynski K., Sim S. A., Hillebrandt W., Fryer C. L., Fink M., Kromer M., 2011, MNRAS, 417, 408

Ruiz-Lapuente P., 2014, New A Rev., 62, 15

Saio H., Nomoto K., 2004, ApJ, 615, 444

Scalzo R. A., Ruiter A. J., Sim S. A., 2014, MNRAS, 445, 2535

Schwab J., Shen K. J., Quataert E., Dan M., Rosswog S., 2012, MNRAS, 427, 190

Segretain L., Chabrier G., Mochkovitch R., 1997, ApJ, 481, 355

Shen K. J., Bildsten L., 2009, ApJ, 699, 1365

Shen K. J., Bildsten L., Kasen D., Quataert E., 2012, ApJ, 748, 35

Shen K. J., Moore K., 2014, ApJ, 797, 46

Soker N., Kashi A., García-Berro E., Torres S., Camacho J., 2013, MNRAS, 431, 1541

Sparks W. M., Stecher T. P., 1974, ApJ, 188, 149

Thompson T. A., 2011, ApJ, 741, 82

Timmes F. X., Swesty F. D., 2000, ApJS, 126, 501

Townsley D. M., Moore K., Bildsten L., 2012, ApJ, 755, 4

Tsebrenko D., Soker N., 2015a. MNRAS, submitted

Tsebrenko D., Soker N., 2015b, MNRAS, 447, 2568

van Kerkwijk M. H., Chang P., Justham S., 2010, ApJ, 722, L157

Wang B., Han Z., 2012, New A Rev., 56, 122

Wang B., Justham S., Han Z., 2013, A&A, 559, A94

Webbink R. F., 1984, ApJ, 277, 355

Whelan J., Iben J. I., 1973, ApJ, 186, 1007

Yoon S.-C., Langer N., 2004, A&A, 419, 623

Yoon S.-C., Langer N., 2005, A&A, 435, 967

Yoon S.-C., Podsiadlowski P., Rosswog S., 2007, MNRAS, 380, 933

Zhou W., Wang B., Meng X., Liu D., Zhao G., 2015, ArXiv e-prints

Zhu C., Chang P., van Kerkwijk M. H., Wadsley J., 2013, ApJ, 767, 164